Astron. Astrophys. 339, 194–200 (1998)

ASTRONOMY AND ASTROPHYSICS

The shape of the unidentified infra-red bands: analytical fit to ISOCAM spectra

F. Boulanger[1], **P. Boisssel**[2], **D. Cesarsky**[1], **and C. Ryter**[3]

[1] Institut d'Astrophysique Spatiale, Université Paris Sud, Bat. 121, F-91405 Orsay Cedex, France
[2] Laboratoire de Photophysique Moléculaire, Laboratoire du CNRS, Université Paris Sud, Bat. 213, F-91505 Orsay Cedex, France
[3] DAPNIA/Service d'Astrophysique, CEA/Saclay, F-91191 Gif Sur Yvette Cedex, France

Received 27 February 1998 / Accepted 1 July 1998

Abstract. Modelling the unidentified infrared dust bands at 6.2 7.7, 8.6, 11.3, and 12.7 μm by Lorentz profiles is shown to produce excellent fits to the spectra obtained with the Continuous Variable Filter (CVF) of the instrument ISOCAM, on-board the Infrared Space Observatory (ISO). The feature pedestals are accounted for by the wide wings of the Lorentz curves which also account for a large fraction of the $10\,\mu$m "continuum". The Lorentz shape of the features is believed to reveal intrinsic properties of the emitters, i.e. a very short life time of the excited state, of the order of a few 10^{-13}s. This is attributed to internal vibrational redistribution (IVR) between thermally accessible modes of the particles, which can be raised at high temperature by absorption of a single photon. Particles of a few hundred atoms may meet both requirements.

Key words: ISM: clouds – ISM: Rho-Ophiuchi cloud – ISM: NGC 7023 – infrared: ISM: lines and bands – infrared: line formation

1. Introduction

The unidentified infrared (UIR) dust bands at 3.3, 6.2, 7.7, 8.6, 11.3, and $12.7\,\mu$m, observed in different kind of celestial nebulae, have been widely attributed to aromatic C-C and C-H bindings in molecules and/or larger particles. Combinations of Polycyclic Aromatic Hydrocarbons molecules (PAHs) have been proposed to account for the observed interstellar features, based on laboratory experiments and quantum mechanical calculations on molecules with sizes up to a few tens of atoms (Léger & Puget 1984, for reviews see Allamandola et al. 1987, Puget & Léger 1989). A good spectral match between the interstellar bands and terrestrial coals with a high degree of aromatic substructures have been demonstrated. In regions of intense radiation fields, such as in proto-planetary nebulae, large solid particles can be hot enough to account for the bands (Guillois et al. 1994).

Thanks to its high sensitivity, the Infrared Space Observatory ISO (Kessler et al. 1996) has enormously added to the knowledge in this field. First, the bands which were implicitly associated with nebulae have been shown to be present in cirrus spectra, where the radiation field is so low that there is no alternative mechanism to the transient heating of small particles by absorption of a single photon (Mattila et al. 1996; Boulanger et al. 1998). Models of emission from a continuous size distribution of particles indicate that the mid-infrared radiation of the ISM is dominated by particles from one hundred to one thousand atoms (Désert et al. 1990, Schutte et al. 1993). Second, spectra obtained at high resolution with the Short Wavelength Spectrometer (SWS, Verstraete et al. 1996, Roelfsema et al. 1996) indicate that the band profiles are smooth with only little suggestion of resolved substructures. Finally, the spectra show emission between the main dust features (Boulanger et al. 1996).

For this work, we have analysed spectra obtained on galactic objects, taken from a program aimed at selecting, as much as possible, simple and uniquely specified physical situations and low extinction. They have been obtained with the rotating Circular Variable Filter (CVF) of the camera ISOCAM (Cesarsky et al. 1996a) on-board the satellite ISO. We discover that the UIR dust bands as displayed by ISOCAM are best represented by Lorentz profiles with wide wings, contrasting with the Gauss profiles which have narrower wings. This paper presents this decomposition of the spectra and discusses its physical signification.

2. Observations

For this analysis we have used CVF observations on the reflection nebula NGC 7023, the Ophiuchus molecular cloud, and the Helix nebula. These data are part of works published elsewhere. For the data description and processing, and details of the observations, we refer the reader to the original papers (Cesarsky et al. 1996b, Boulanger et al. 1998, Cox et al. 1998).

Subtraction of the zodiacal emission is an aspect of the data reduction which is of importance for the analysis presented in this paper. For this subtraction we made use of the zodiacal spectrum obtained with ISOCAM on a blank piece of sky (Reach et al. 1996). We used data from the Diffuse Infrared Background Experiment (DIRBE, Boggess et al. 1992) to estimate the ratio of zodiacal emission intensities of the Ophiuchus and Reach et al. observations. The main uncertainty in this pro-

Send offprint requests to: F. Boulanger

cedure is set by the reproducibility of the ISOCAM detector response between two independent observations. The comparison of DIRBE data with ISOCAM observations of uniform high latitude fields shows that this uncertainty is smaller than 20%.

NGC 7023, one of the most extensively studied reflection nebulae, is a reference object for the study of the UIR bands (Sellgren et al. 1985). It is illuminated by the Herbig B3Ve star HD 200775 at a distance of 440 pc (Whitcomb et al. 1981). The ISOCAM spectrum presented in Fig. 1 is taken form the data presented by Cesarsky et al. (1996b) at a position within the bright emission ridge to the north of HD 200775. The ultraviolet radiation field at this position is estimated to be about 1000 the solar neighborhood value, $\mathrm{u}_0 \sim 0.13\,\mathrm{eV\,cm^{-3}}$ (Mathis et al. 1983).

The Rho-Ophiuchi molecular cloud at a distance of 150 pc is a favored target for star formation and interstellar medium studies. The field of our observation (3'x3' centered at $\alpha(2000)$ =16:25:52.2 $\delta(2000)$ =-24:19:08), 10 armin N-E of the exciting star HD147889 (B2 IV), is located in the western Photo-Dissociation Region (PDR) of the main molecular cloud (Abergel et al. 1996). Neglecting projection effects and extinction, an upper limit on the ultraviolet radiation density is $\mathrm{u} \sim 10\,\mathrm{eV\,cm^{-3}}$, or ~ 60 times the solar neighborhood value. We extracted from the data one spectrum which is displayed in Fig. 1.

The gaseous envelope of the Helix, an old planetary nebula, was found to be dominated by several gas lines from H_2 and ions, with no UIR bands (Cox et al. 1998). It is thus an appropriate object to calibrate the instrumental resolution and spectral profile of the ISOCAM CVF. Fig. 2 shows a high signal to noise spectrum of the S(5) H_2 line which is very well fitted by a Gaussian profile. The full-width at half-maximum (FWHM) derived from this fit and those of other lines are given in Table 1. CVF spectral images are obtained by scanning step by step the wavelength. The CVF spectra can thus be affected by memory effects of the ISOCAM detector. For the three data sets, we corrected, to a good approximation, these memory effect by using the procedure described in Abergel et al. (1996). Our confidence that the analysis presented here does not suffer from residual memory effects comes from the two following facts. (1) The Helix and Ophiuchus observations were both performed by going from long to short wavelengths and the gas lines in the Helix observation show no asymmetry that would indicate a residual memory effect (see Fig. 2). (2) The NGC 7023 observation was performed by scanning both up and down in wavelength. In the final spectra, the shape of the dust features are identical in the two scan directions.

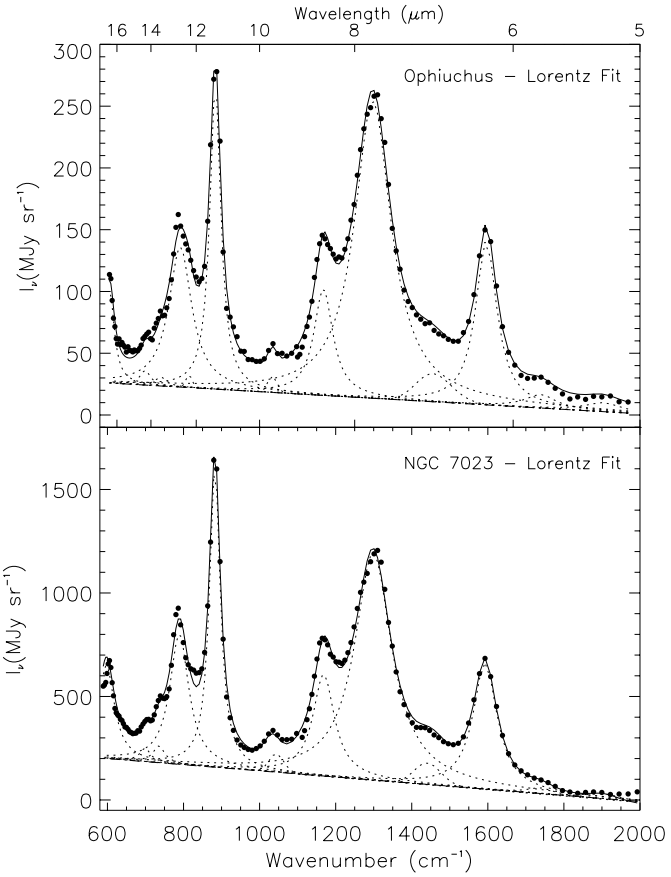

Fig. 1. ISOCAM CVF spectra for one pixel in the NGC 7023 reflection nebula ($\alpha(2000)$ =21:01:36.1 and $\delta(2000)$ =68:10:46) and another pixel in the Rho-Ophiuchi molecular cloud ($\alpha_{2000} = 16:25:47.3$, $\delta_{2000} = -24:18:57$). The spectra are fitted by a set of 9 Lorentz profiles plus two Gaussian lines associated with the S(3) and S(5) H_2 rotational lines (see Sect. 3.1). The symbols are dots for data points, dashed lines for the elementary Lorentz profiles, and solid line for the resulting fit. The linear base used in the fit is shown as a dashed line.

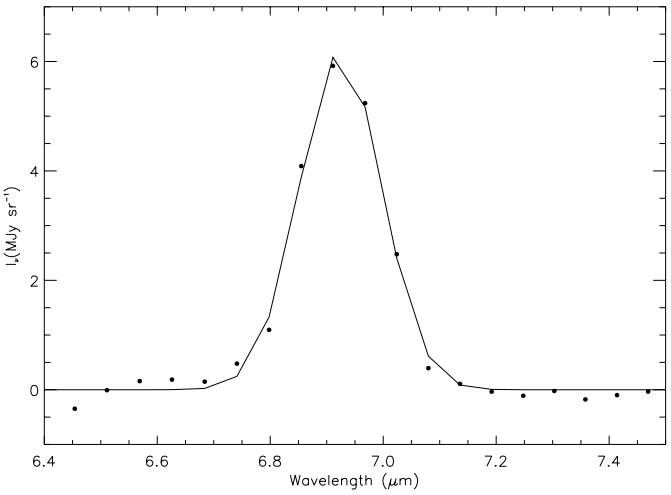

Fig. 2. One example of a Gaussian fit to the S(5) H_2 line in the Helix Nebula observations (Cox et al. 1998). Similar fits were used for the spectral calibration of the CVF (see Table 1).

3. Analysis of dust bands

3.1. Analytical fit of the spectrum

Fig. 1 intuitively suggests that the NGC 7023 and Ophiuchus spectra are composed of overlapping Lorentzian profile, i.e. with relatively narrow peaks but wide wings, in evident contrast to

Table 1. Gaussian fits to gas lines in the Helix spectrum

Line	λ μm	FWHM μm	FWHM cm^{-1}	$\Delta\nu/\nu$
H2 S(7)	5.51	0.136	45	40
H2 S(5)	6.9	0.163	34	42
H2 S(4)	8.0	0.223	35	36
H2 S(3)	9.66	0.270	30	36
Ne III	15.6	0.332	14	47

the narrow profiles of the gaseous lines of Fig. 2. The Lorentz function is given by:

$$\mathrm{F}(\nu) = \mathrm{A} \times \mathrm{f}(\nu) \quad (1)$$

where

$$f(\nu) = (1/(\pi \times \sigma)) / \left(1 + (\nu - \nu_0)^2/\sigma^2\right) \quad (2)$$

is the normalized Lorentz profile. Here ν is the frequency, ν_0 the position of the band, σ its width parameter. The peak amplitude of the band is given by $\mathrm{y} = \mathrm{A}/(\pi \times \sigma)$. It follows that its integrated intensity, A, is simply given by

$$\mathrm{A} = \pi \times \mathrm{y} \times \sigma = (\pi/2) \times \mathrm{y} \times \mathrm{FWHM} \quad (3)$$

where $\mathrm{FWHM} = 2\sigma$ is the full width at half maximum. If the Lorentzian shape of the bands has a physical signification, it must be expressed as a function of the frequency instead of the wavelength. This is why we chose to display the spectra as a function of the wave number (in cm^{-1}), in the spectroscopic tradition. However, in the text we shall refer to the individual features by their wavelength in μm, which are probably more familiar to most astronomers in the field.

We started to fit the spectrum with a set of six Lorentz profiles at frequencies 1602, 1300, 1173, 886, 797 and $605\,\mathrm{cm}^{-1}$ (Eq. (1)) corresponding to the main bands at 6.2, 7.7, 8.6, 11.3, 12.7 and $16.5\,\mu$m. A linear baseline had also to be introduced. The $16.5\,\mu$m band is at the extreme limit of the observed spectral range and only half of it is seen in the Ophiuchus observation. For this last feature we fixed the central wavelength and width, and fitted only the intensity. Minor bands or lines at 1923, 1724, 1445, 1031, and $709\,\mathrm{cm}^{-1}$ (5.2, 5.8, 6.9, 9.7, $14.1\,\mu$m) are also present in the data. We fitted the minor features in the residuals of the first fit. The 6.9 and $9.7\,\mu$m lines coincide with the S(5) and S(3) H_2 lines, which have been adjusted by Gaussian profiles. The three other lines which are probably dust features with an intensity a few percent of that of the main bands have been adjusted with Lorentz profiles. The complete fit with all the features of the NGC 7023 and Ophiuchus spectra are presented in Fig. 1. The automatic adjustment of the six main bands and the linear baseline provides a good fit to the spectrum. An even closer fit was obtained with the additional features. Intensities and widths of the main bands derived from this fit are given in Table 2.

Note that the wings completely account for more than half of the signal in the spectrum valley around $10\,\mu$m. The remaining signal (18% of the total power over the 5 to $16.5\,\mu$m wavelength range) is accounted for by the linear baseline which represents a true signal and is not instrumental. For Ophiuchus, at $12\,\mu$m the baseline intensity represents 50% of the zodiacal emission which has been subtracted from the ISOCAM spectrum (Sect. 2). It is thus significantly larger than our uncertainty on the zodiacal light subtraction estimated to be at most 20%. In NGC 7023 where the baseline intensity is about five times higher, this argument is even stronger. The linear baseline is not necessarily a true continuum emission. It could represent the sum of a set of numerous weak features which are not resolved with the CVF resolution. Analysis of high signal to noise spectra should allow to test this hypothesis at least in bright objects.

Gaussian and Lorentzian fits to the Ophiuchus spectrum are compared in Fig. 3; the small features have been removed to leave only the six main dust bands. The Gaussian fit is as good as the Lorentzian fit only if, in addition to the six UIR bands and the linear continuum, we allow for two broad components at about 840 and $1375\,\mathrm{cm}^{-1}$ (11.9 and $7.3\,\mu$m), thus six additional parameters. Without these broad components the gaussian fits fail in accounting for the signal at the edge of the bands. In this decomposition the broad Gaussian components and the linear baseline include 60% of the total power integrated from 5 to $16.5\,\mu$m while the baseline represents only 18% of this total power for the Lorentzian fit. Our preference for the Lorentz fit is also motivated by the physics of the emission from large molecules at high temperature (Sect. 4.2). In the following we focus on the interpretation of the Lorentz fit.

3.2. Effect of the CVF finite resolution

3.2.1. Voigt profiles

For the narrowest bands, the width derived from the Lorentz fits is not much larger than the spectral resolution. We assessed the effect of the finite resolution of the CVF (as interpolated from Table 1) on the bands profiles as follows. The convolution of a Gauss and a Lorentz profile is known as a Voigt profile (e.g. Lang 1980). The Voigt fitting algorithm may not properly converge for a large set of features. Thus, as in Fig. 3, the minor bands have been subtracted from the spectrum before fitting. The result is displayed in Fig. 3, with the same line styles as in Fig. 1.

As can be seen, the synthetic spectrum obtained with the Voigt procedure fits very properly the observations. It proves that the bands are intrinsically well fitted by Lorentz profiles and that the wings of the features are not produced by the finite resolution of the CVF. The intensities and deconvolved widths obtained with the Voigt fit are listed in Table 2. The intensities derived with the Lorentz and Voigt fitting procedures are very close to each other as it should be; the 10% difference observed for the 12.7 and $11.3\,\mu$m features is very probably due to the tight overlapping of the bands, which makes the separation of the respective contribution of the two bands somewhat uncertain. The fact that the amplitude differences are in opposite directions and average close to zero supports this interpretation.

Table 2. Lorentz and Voigt fits to the Ophiuchus and NGC 7023 spectra

λ	12.7 μm 787 cm^{-1}	11.3 μm 885 cm^{-1}	8.6 μm 1160 cm^{-1}	7.7 μm 1300 cm^{-1}	6.2 μm 1610 cm^{-1}
Ophiuchus					
A(Lorentz)[1]	4.0	4.0	2.3	13.4	4.3
A(Voigt)[1]	4.3	3.5	2.1	13.2	4.0
FWHM(cm^{-1})[2]	73	34	57	119	70
FWHM(cm^{-1})[3]	73	23	44	113	55
NGC 7023					
A(Lorentz)[1]	19	24	16	61	21
FWHM(cm^{-1})[2]	65	34	69	118	73

(1) Intensities of the bands($10^{-6}\mathrm{Wm}^{-2}\mathrm{sr}^{-1}$) obtained with the Lorentz and Voigt fitting procedures.
(2) Full width at half maximum for the Lorentzian fit.
(3) True (deconvolved) width from the Voigt fitting procedure.

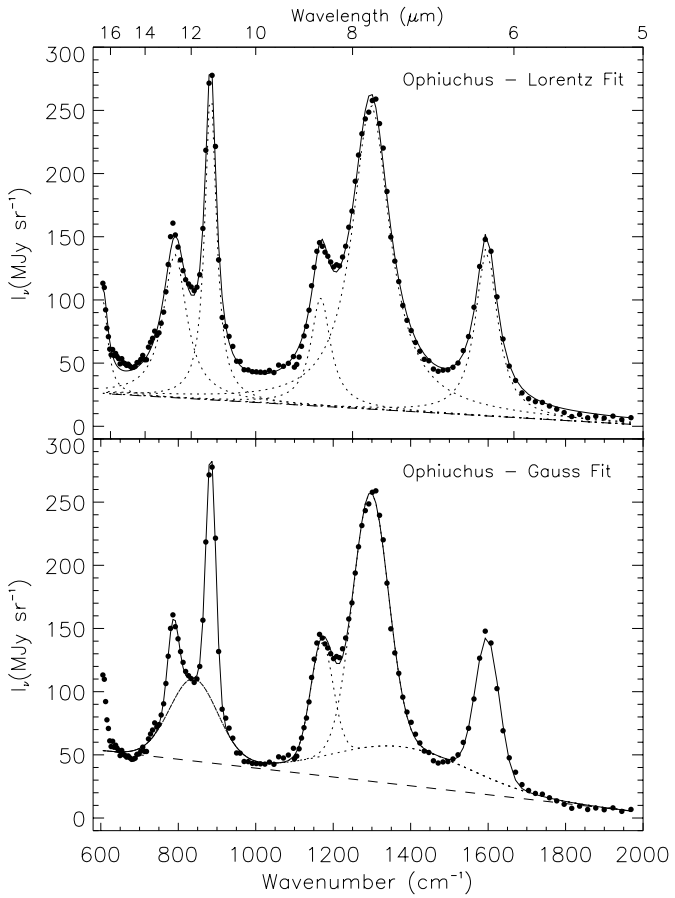

Fig. 3. Comparison of the Lorentzian and Gaussian fits for the Ophiuchus spectrum. The symbols are the same as in Fig. 1. The small dust features and gas lines have been subtracted from the spectra of Fig. 1.

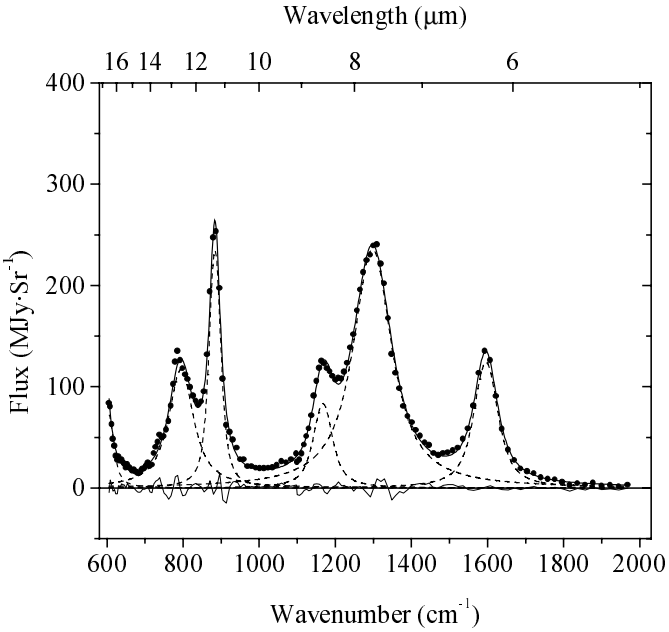

Fig. 4. The main bands fitted by Voigt profiles (Lorentz profiles convolved by the instrument resolution, see Sect. 3.2.1 for details). The symbols are the same as in Fig. 1. The minor bands and the linear baseline of Fig. 1 have been subtracted from the data.

For the three narrowest features (6.2, 8.6 and 11.3 μm) the intrinsic band widths derived from the Voigt fit are appreciably smaller than the values derived from the initial Lorentzian fit which shows that the instrumental convolution affects the spectral shape of the peak. Nevertheless, the fact that globally the fit is better with Lorentz than with Gauss profiles shows that, for all band wings, the intrinsic Lorentz shape dominates the instrumental broadening as well as any intrinsic broadening.

In conclusion, we propose that the Lorentz fit to the UIR bands provides an unequivocal method to properly separate the different components of the infrared emission, and should clarify the respective roles played by the underlying continuum and the features themselves. A first good approximation is already obtained with the six main features. Refinement is gained by adding the weaker bands. The problem of choosing appropriate baselines to compute the intensity of each band is also eliminated. An important result of our analysis is that a large fraction of the power emitted between the features belongs to the bands themselves. In other words, the quantities $\mathrm{A_i}$ listed in Table 2

represent the true intensity of the UIR bands, which would be grossly underestimated if measured with Gaussian fits. We note in passing that, although the physical processes involved are certainly different, this procedure is reminiscent of that propose by Fitzpatrick & Massa (1990) to quantify the UV extinction bump by a Drude profile, which is a modified Lorentz profile.

3.2.2. Comparison with SWS Observations

Higher resolution spectra have been obtained on a wide variety of objects with the Short Wavelength Spectrometer (SWS). Many published spectra such as those of the M17 H II - molecular cloud interface (Verstraete et al. 1996), compact H II regions (Roelfsema et al. 1996, 1998) and circumstellar envelopes (Molster et al. 1996) refer to objects with a very high radiation field. In such environments very small grains (VSGs) heated by the absorption of several photons contribute to the mid-IR emission. It is thus not straightforward to compare these data with the spectra, presented in this paper, obtained in regions where the VSGs are not hot enough to radiate in the ISOCAM wavelength range. An additional problem to bear in mind is that, in molecular clouds with very large column density like that associated with M17 and compact H II regions, the spectrum shape and the level of the signal around $10\,\mu$m may be significantly affected by extinction and in particular the silicate $9.6\,\mu$m feature. Thus, high radiation field objects are not best suited to study the emission properties of the smallest dust particles.

More recently, Moutou et al. (1998) published an SWS spectrum of NGC 7023. Fig. 1 of this paper shows that the feature pedestals and the $10\,\mu$m continuum are present in the SWS data as in the ISOCAM spectra. The NGC 7023 SWS spectrum, when displayed as a function of wavelength, shows some asymmetry of the 6.2 and $11.3\,\mu$m features, with larger wings on the red side. Note that a resonance curve is symmetrical as a function of the frequency (or wave number), but trails towards the red when displayed as a function of wavelength. This effect increases with the width of the line and is not completely negligible for the mid-infrared UIB features. In the Lorentz decomposition some asymmetry of the 6.2 and $11.3\,\mu$m is introduced by the underlying wings of the 7.7 and $12.7\,\mu$m features. However, these two effects do not entirely account for the asymmetry observed in the SWS spectra. By looking carefully at the Lorentz fits in Fig. 1, one can see that the blue side of the $11.3\,\mu$m band is slightly narrower than the fit. A combination of Lorentz functions would thus be necessary to account for the asymmetry.

It has also been known for some time that the "$7.7\,\mu$m" feature is composed of at least two components, at wavelength of about 7.6 and $7.8\,\mu$m respectively, with varying relative intensities (Bregman 1989; Roelfsema et al. 1996). This appears clearly in the SWS spectra and can also be seen in the ISOCAM data. The single component (Lorentzian or Gaussian) fit of the $7.7\,\mu$m feature do not provide a good fit at the peak of the band. In Fig. 5, we show that a better fit is obtained with two bands at 7.6 and $7.8\,\mu$m. We stress that the fact that we replaced one broad component by two slightly shifted components does not affect the ability of the Lorentz profiles to account for the wings.

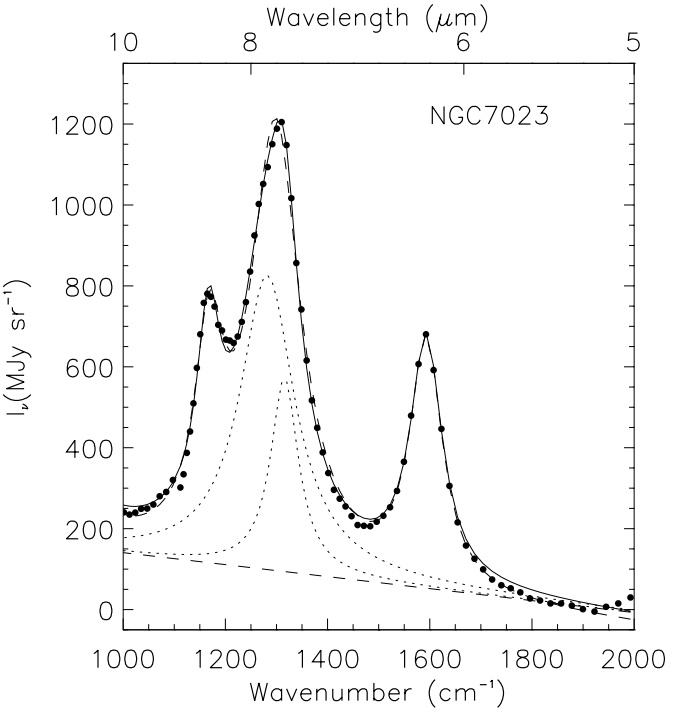

Fig. 5. Fit of the $7.7\,\mu$m dust feature with two Lorentz profiles (solid line). The fit with one single $7.7\,\mu$m component is shown as a dash line. The 7.6 and $7.8\,\mu$m Lorentz profiles for the two components fit are shown with dotted lines. The minor features and gas lines have been subtracted from the data as in Fig. 3

The SWS data clearly show that the true band shape must be a combination of Lorentz profiles with different central frequencies and widths; this is particularly obvious for the 7.7 and $12.7\,\mu$m features the peaks of which are not well fitted by a single Lorentz profile (Fig. 3 and 5). The combination is important to fit the emission peaks but has little effect on the width and intensity of the band wings, which contain more than half of the total radiated power. Physically, it is not unexpected to observe a combination of Lorentz profiles since the width and position of the features may vary from particle to particle and with temperature (Sect. 4).

4. Discussion

The two spectra presented in Fig. 1 are believed to represent a typical case of mid-IR emission bands from carbon particles, and will be be taken as representative for interstellar environments with moderate radiation energy density (up to 10^3 times the solar value).

4.1. Physical significance

The fact that the UIR bands are well described as wide Lorentz profiles can be related to the physics of the emission of large molecules at high temperature. We propose that the observed width, in the range of 20 to 100 cm^{-1} (a fraction of a micron) is largely due to intramolecular broadening processes. When

a high amount of energy is present in a large molecule, the exchange of excitation between the accessible modes is very fast (Barker et al. 1987). This process, known as Internal Vibrational Redistribution (IVR) occurs with characteristic time scales that can be shorter than 10^{-13} s. The excited levels of a given vibrational mode are continuously populated and emptied by non-radiative transfer to the other modes. The width of the transition reflects the short time between such events. Note that this time is incommensurate with the radiative cooling time generally quoted for PAHs, which is of the order of seconds or more (Léger & Puget 1984).

4.2. Laboratory support

The broadening of energy levels by IVR has been demonstrated by laboratory observations. Ionov et al. (1988, see also references therein) have shown that the 935 cm-1 ($10.7\,\mu$m) transition of the $(CF_3)_3Cl$ molecule excited at 36500 and 42500 cm^{-1} (4.3 and 5.3 eV) exhibits Lorentzian shapes corresponding to life-times of $6.2\,10^{-13}$ and $4.3\,10^{-13}$ s. This experiment also shows that the central frequency and width of the energy transition varies with the internal temperature. Closer to the astrophysical observations, Joblin et al. (1995) have found that the bands in spectra of PAHs, such as coronene at temperatures of about 700 K, have widths in the range 10–30 cm^{-1}. These widths, much larger than those measured for PAHs in cryogenic matrices, increase with temperature in agreement with what is described by Ionov et al. (1988). For the $3.3\,\mu$m line, the extrapolation of the temperature dependence allows to connect the data of Joblin et al. to that of Shan et al. (1991), and Brenner & Barker (1992) on smaller PAHs heated by laser pulses. For coronene at a temperature of ~ 700 K, the 6.2 and 8.6 μm features widths are only a factor 2 to 3 narrower than the interstellar bands (Joblin et al. 1995). The 7.7 and $12.7\,\mu$m features are obviously more complicated; the interstellar $7.7\,\mu$m band appears as a combination of at least two modes (Sect. 3.2).

Since the lines of individual PAHs studied in the laboratory are spread about the interstellar bands, the interstellar spectra may result from the combination of emission from numerous molecules. However, it is most unlikely that the Lorentz shape could result from a random combination of narrower lines. We rather think that to a large extent the width of the emission bands is intrinsic to the emission of each particle and is larger than that measured, in the laboratory, for PAHs with less than a few tens of atoms.

Models built to account for the spectral energy distribution of dust emission in the near and mid-IR show that only the emission in the $3.3\,\mu$m comes from molecules with less than ~ 50 atoms. For a continuous size distribution between these molecules and dust grains, the emission in the $6.2\,\mu$m and longer wavelength features comes from particles with up to several hundred atoms, one order of magnitude larger than the PAHs studied in the laboratory (Désert et al. 1990, Schutte et al. 1993). We are not aware of any theoretical or experimental work on such large particles. In relation with our interpretation of the width of the bands, we can only speculate that for large particles, the larger number of accessible modes makes the internal exchange faster, the life-times shorter and the bands wider. Our interpretation of the spectra also requires that for such large particles the vibrational modes do not depend much on the exact shape of the particle. The positions of the emission lines of PAHs around 6.2 and $7.7\,\mu$m depend strongly on the type of the molecule (e.g. Léger & d'Hendecourt 1987). This is due to the fact that these bands correspond to in-plane C-C vibrational modes of the hexagonal lattice, which are strongly affected by boundary effects. In small molecules, asymmetries and irregularities of the shape induce the various line shifts and splittings between 6 and $8\,\mu$m. In large particles, boundary effects become relatively less important and indeed, measurements by Friedel & Carlson (1971) show that a broad infrared emission feature exists around $7.7\,\mu$m in finely ground graphite. Raman spectroscopy of graphite by Tuinstra & Koenig (1970) reveals the same effect. Interpolating between these two extremes situations, small molecules and graphite particles, it is tempting to speculate that PAHs of a size intermediate between molecules and VSGs (Désert et al. 1990) may reconcile the observations. We note that such large particles, such as polymeres of coronene up to $C_{96}H_{36}$, and graphenes up to about 250 C-atoms, have been recently produced and detected in the laboratory (Joblin et al. 1997). The combination of the 7.6 to $7.8\,\mu$m lines would be a remote consequence of relatively small boundary effects in those large particles.

5. Conclusion

The main results of our analysis of the spectral shape of the mid-IR interstellar emission can be summarized as follows.

(1) The fitting of the carbon dust bands by Lorentzian profiles provides an unequivocal and hopefully universal way to quantify and separate the different components of the celestial unidentified mid-infrared dust spectra. The wide wings of the Lorentz profiles account for the broad pedestals of the bands. The true intensity is grossly underestimated if these wings are ignored. A continuum remains necessary but it has a simple linear shape.

(2) It is most unlikely that the Lorentz shape could result from a random combination of many lines. We think that, to a large extent, the width of the UIR is intrinsic to the emission of each particle.

(3) We propose to associate the width of the Lorentz profiles to the life-time of the emitting level. The very short life-time corresponds to the duration of the excitation of a given vibrational mode before the energy is internally transferred to another mode through internal vibrational redistribution (IVR). This interpretation is supported by laboratory data on infrared transitions from large molecules at high temperature. We consider that this work provides further support to one key aspect of the PAH hypothesis, namely that the carriers of the bands are heated by the absorption of single photons.

Acknowledgements. ISO is an ESA project with instruments funded by ESA Member States and with the participation of ISAS and NASA.

References

Abergel, A., Bernard, J.P., Boulanger, F., et al. 1996, A&A 315, L329

Allamandola, L.J., Tielens, A.G.G.M., Barker, J.R., 1987, Infrared Emission From Interstellar PAHs, in: Morfill, G.E. and Scholer, M. (eds) Physical Processes in Interstellar Clouds, Reidel (Nato series), Dordrecht, p. 305

Barker, R.J., Allamandola, L.J., Tielens, A.G.G.M., 1987, ApJ 315, L61

Boggess, N., Mather, J.C., Weiss, R., et al. 1992, ApJ 397, 420

Boulanger, F., Reach, W.T., Abergel, A., et al., 1996, A&A 315, L325

Boulanger, F., Abergel, A., Bernard, J.P., et al. 1998, in Star Formation with ISO, eds. J. L. Yun and R. Liseau, Astronomical Society of the Pacific, San Francisco, p. 15

Bregman, J.D. 1989, Observations of HII Regions and Planetary Nebulae: The Infrared Emission Bands. in: Allamandola,L.J. and Tielens, A.G.G.M. (eds) Interstellar Dust, IAU Symp. 135, Kluwer, Dordrecht, p. 109

Brenner, J.D., Barker, J.R., 1992, ApJ 388, L39

Cesarsky, C.J., Abergel, A., Agnèse, P., et al., 1996a, A&A. 315, L32

Cesarsky, D., Lequeux, J., Abengel, A., et al., 1996b, A&A 315, L305

Cox, P., Boulanger, F., Huggins, P.J. et al., 1998, ApJ 495, L23

Désert, F.X., Boulanger, F., Puget, J.-L. 1990, A&A 237, 215

Fitzpatrick, E.L., Massa, D., 1990, ApJ suppl. 72, 163.

Friedel, R.A., Carlson, G.L., 1971, J. Phys. Chem.15, 1149

Guillois, O., Nenner, I., Papoular, P., Reynaud, C., 1994 A&A 285, 1003

Ionov, S.I., Stuchebryukhov, A.A.,Bagratashvili, V.N. et al., 1988, Appl. Phys. B 47, 229

Joblin, C., Boissel, P., Léger, A., d'Hendecourt, L., Défourneau, D., 1995, A&A 299, 835

Joblin, C, Masselon, C., Boissel, P. et al., 1997, Rapid. Com. M. Spectr. 11, 1619

Kessler, M.F., Steinz, J.A., Anderegg, M.E., et al., 1996, A&A 315, L27

Lang, K.R., 1980, Astrophysical Formulae, Springer Verlag, Berlin, p. 219

Léger, A., d'Hendecourt, 1987, Identification of PAHs In Astronomical IR Spectra-Implications in: Léger, A., d'Hendecourt, L., Boccara, N. (eds) Polycyclic Aromatic Hydrocarbons and Astrophysics, Reidel (NATO series), Dordrecht, p. 223

Léger, A., Puget, J.-L., 1984, A&A 137, L5

Mathis, J.S., Mezger, P.G., Panagia, N., 1983, A&A 128, 212

Mattila, K., Lemke, D., Haikala, L.K., et al., 1996, A&A 315, L353

Molster, F.J., van den Anker, M.E., Tielens, A.G.G.M., et al. 1996, A&A 315, L373

Moutou, C., Sellgren, K., Léger, A., et al. 1998, in Star Formation with ISO, eds. J. L. Yun and R. Liseau, Astronomical Society of the Pacific, San Francisco, p. 47 247

Puget, J.-L. Léger, A., 1989, Ann. Rev. A. Ap. 27, 161

Reach, W.T., Abergel, A., Boulanger, F., et al. 1996, A&A 315, L381

Roelfsema, P.R., Cox, P., Tielens, A.G.G.M., et al., 1996, A&A 315, L289

Roelfsema, P.R., Cox, P., Kessler, M.F., Baluteau, J.-P., 1998, in Star Formation with ISO, eds. J. L. Yun and R. Liseau, Astronomical Society of the Pacific, San Francisco, p. 76.

Sellgren, K., Allamandola, L.J., Bregman, J.D., Werner, M.W., Wooden, D.H. 1985, ApJ 299, 416

Shan, J., Suto, M., Lee, L.C., 1991, ApJ 383, 359

Schutte, W.A., Tielens, A.G.G.M., Allamandola, L.J., 1993, ApJ 415, 397

Tuinstra, F., Koenig, J.L., 1970, J. Chem. Phys. 53, 1126

Verstraete, L., Puget, J.-L., Falgarone, E., et al., 1996, A&A 315, L337

Whitcomb S.E., Gatley, I., Hildebrand, R.H., Keene, J., Sellgren, K., Werner, M.W. 1981, ApJ 246, 416